Desalination and Water Treatment
www.deswater.com
doi: 10.5004/dwt.2023.29427

290 (2023) 217–225
April

Dynamic feature extraction of flood disaster data based on improved Gabor wavelet transform

Wenbing Jiang

School of Urban Economics, Lanzhou City University, Lanzhou 730070, China, email: jld091720@163.com

Received 2 April 2022; Accepted 19 July 2022

ABSTRACT

The data classification effect is poor and the loss of data is large in the process of extracting dynamic features of flood and waterlogging disaster data. A two-dimensional mathematical model of flood routing is constructed based on mobile group intelligence network, the boundary conditions and parameters of flood and waterlogging region were set, and flood and waterlogging data were dynamically collected. The experimental results show that the proposed method has high fitting degree between initial stroke width and actual stroke width, low loss rate of positive samples and good application effect.

Keywords: Gabor filter; Wavelet transform; Flood disaster; Feature extraction

1. Introduction

Flood and waterlogging is the most common and harmful one among all kinds of natural disasters [1]. The floods, which occur frequently, spread widely, are turbulent and extremely destructive, not only inundating houses and populations, causing massive human casualties, but also sweeping away all items from human settlements, including food, and flooding farmland, destroying crops, leading to a significant reduction in food production, resulting in famine. Floods can also destroy factories, factories, communications and transportation facilities, causing damage to the national economy. China has been a country with serious flood disasters since ancient times. China has a vast territory, complex terrain and remarkable monsoon climate. It is one of the countries with frequent floods and wide impact. Flood and waterlogging are a long-term disaster in China. Rainstorm and typhoon disasters are frequent in all regions due to abnormal climate, and rainy seasons are concentrated and changeable. Frequent occurrence of concentrated precipitation in some regions leads to a large amount of accumulated water within a short time. At the same time, due to the restriction of natural conditions and social and economic conditions, accumulated water cannot be discharged in a timely manner, resulting in the destruction of houses, submergence of farmland, erosion of dikes and dams, damage to public infrastructure, etc. Flood disaster not only causes economic losses and casualties, but also seriously affects people's normal life. Therefore, in order to reduce and avoid the loss, let people know the real-time situation of the disaster in time, and avoid the unnecessary loss caused by the lack of pre-disaster warning and forecasting information, it is necessary to establish an appropriate and effective flood warning model, in which the dynamic feature extraction of flood disaster data can provide help for flood warning [2].

Li [3] through the 3D extension module of ArcGIS, the process of reservoir inundation evolution is analyzed, and the dynamic process of flood inundation is further restored, so the scene simulation of flood is realized, and the 3D flood is analyzed and discussed more deeply, but the data classification effect is poor. Zhao et al. [4] set up the real-time flood control operation model of Hekou Reservoir with the maximum peak shaving rate as the goal, put forward the method of using the flood control storage capacity in stages and dynamically, select the historical flood and the

100-y infrequent flood process of Hekou Village Reservoir, and through the real-time forecast operation simulation, determine the upper limit of the dynamic control value of the flood limit water level of Hekou Village Reservoir to be 250 m under the condition of ensuring sufficient safety margin, and increase the average flood resource utilization amount of multiple floods by 4,070 × 104 m^3 without increasing the flood control risk, but its data loss is large.

This paper studies the dynamic feature extraction method of flood disaster data based on the improved Gabor wavelet transform in view of the disadvantages of the above methods, and improves the Gabor wavelet transform algorithm to extract the corresponding dynamic feature of Gabor flood disaster data.

2. Dynamic collection and pre-processing of flood disaster data

2.1. Dynamic data collection of two-dimensional flood routing mathematical model

There are many methods to simulate flood routing because of the difference of flood disaster. However, most of the current numerical simulation methods are concentrated in the river flood and flood storage and detention areas and so on. In the process of flood routing, the dry and wet boundary often changes, and the corresponding mathematical model is constructed mainly by the characteristics of flood routing. The corresponding 2-D shallow water equations are discretized in order to simulate the process of 2-D flood routing, and the corresponding terrain elevation data are provided by the mobile group intelligence perception network platform, dynamic collection of flood disaster data by two-dimensional flood routing mathematical model is realized.

The mobile group intelligence awareness network consists of a base station server and several child nodes. The model structure is shown in Fig. 1.

Each node can communicate with the server for data information. Specifically, the user mobile terminal device is a child node, the server is responsible for data integration and analysis, through wireless and wired communications to form a sensing network. In order to ensure the security of data privacy, the sub-nodes are not connected to each other, and their data can only be kept by themselves [5–7].

- Establishment of remote sensing image database. Through the ParGIP parallel remote sensing image processing software developed by ourselves, the remote sensing image of the studied area is corrected and inlaid, and the image is classified, so as to get the actual situation of the studied area before the disaster, and prepare for the subsequent image fusion and the extraction and processing of water body residents. The Parallel Geographic Image Processing Model (ParGIP) consists of eight PCs with main frequency of 400 MB, memory of 256 MB and one Switch to form a cluster Ethernet, LINUX11112 operation model, and AJJIIA development platform based on distributed memory sharing. In this way, we can use the software of ParGIP to use the large scale topographic map to select the points of the same name to form the ground control point, and then correct and register the pre-disaster remote sensing images.
- Establishment of vector database of basic geographic elements (water body, terrain, administrative division, etc.). The binary raster data such as water and land use obtained from remote sensing image data through classification are first converted to Grid format and then to vector formatin ArcINFO.

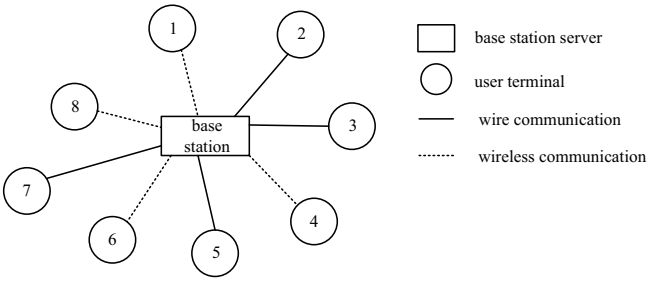

Fig. 1. Mobile swarm intelligence perception network model.

Suppose that there are n user terminals in the mobile swarm intelligence sensing network, that is, there are n sub nodes, and each sub node a^i contains I data a^i_m, which can be expressed as:

$$a^i = \left\{a^i_1, a^i_2, \cdots, a^i_m\right\} \tag{1}$$

In the data center, the data a^i_m of each sub node is further divided into several items, which are represented as:

$$a^i_m = \left\{b^j_{1i}, b^j_{2i}, \cdots, b^j_{ni}\right\}, \left(2 \le n \le m\right) \tag{2}$$

Among them, b^j_i must satisfy the following conditions:

$$\sum_{l=1}^{n} b^j_{li} = a^i_m \tag{3}$$

In Eq. (3), b^j_{li} is any positive real number. The sub node data can be transformed into data slicing:

$$a^i_m = \begin{bmatrix} b^j_{11} & b^j_{12} & \cdots & b^j_{1l} \\ b^j_{21} & b^j_{22} & \cdots & b^j_{2l} \\ \cdots & \cdots & \cdots & \cdots \\ b^j_{n1} & b^j_{n1} & \cdots & b^j_{nl} \end{bmatrix}_{n\times l} = A_{1\times n} B^j_{n\times l} \tag{4}$$

In Eq. (4), $A_{1\times n}$ represents a n dimensional row vector, and the g-th row in $B^j_{n\times l}$ is B^j_g, representing a data slice, that is, a matrix:

$$B^j_g = \left[b^j_{g1}, b^j_{g1}, \cdots, b^j_{gl}\right]_{1\times l} \tag{5}$$

The remaining n–1 data slices are randomly distributed to any sub nodes in the network. After all the distributed data slices are received by all the sub nodes, the data slices

U^j are mixed and transmitted to the base station server to complete the data collection.

Fluid flow phenomenon exists in many engineering fields, and the whole process is governed by the basic laws of energy conservation and momentum conservation. Through flood numerical simulation, we can build a mathematical model to reflect the corresponding problems, obtain accurate calculation methods, solve them through experiments, and obtain the best calculation results, Fig. 2 shows the solution process of flood routing model.

In Fig. 2, boundary conditions can be divided into two categories, namely physical boundary and numerical boundary. The setting of each parameter is also different due to the difference of mesh generation method and discrete method. Different parts need to be organically combined to form a whole in order to ensure the smooth construction of the model. The evolution of flood in plane is described by shallow water equation. The basic equation includes continuity equation and momentum equation [8–10], in which Carioles force and wind stress are ignored, which can be expressed in the following form:

$$S = \frac{\partial h}{\partial t} + \frac{\partial q_x}{\partial x} + \frac{\partial q_y}{\partial y} \tag{6}$$

$$0 = \frac{\partial q_x}{\partial t} + \frac{\partial \left(u q_x\right)}{\partial x} + \frac{\partial \left(v q_x\right)}{\partial y} + gh\frac{\partial Z}{\partial x} + g\frac{n^2 u\sqrt{u^2+v^2}}{h^{1/3}} \tag{7}$$

$$0 = \frac{\partial q_y}{\partial t} + \frac{\partial \left(u q_y\right)}{\partial x} + \frac{\partial \left(v q_y\right)}{\partial y} + gh\frac{\partial Z}{\partial y} + g\frac{n^2 u\sqrt{u^2+v^2}}{h^{1/3}} \tag{8}$$

Among them, h is water depth, g is gravity acceleration, t is time, q_x and q_y are flux vectors in x and y directions, respectively, S is source term, u and v are components of flow velocity in x and y coordinate directions in plane space, respectively, n is Manning roughness coefficient.

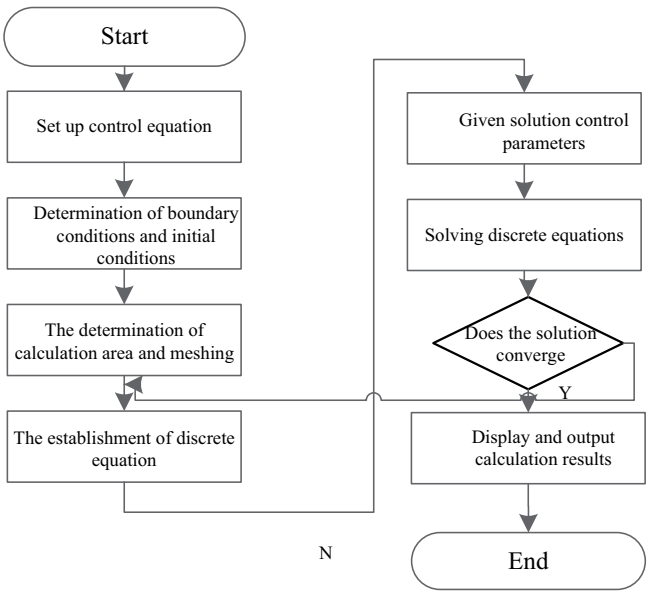

Fig. 2. Two-dimensional mathematical model of flood routing.

In the process of simulating calculation of flood routing, it is necessary to define the area to be calculated and divide it into networks, which is the precondition of simulating calculation. Calculation of the division of the region to ensure that it is continuous, in which the flow of water through the region to be divided into its whole calculation of the region [11–12]. Considering the size of the computational region, if we select too large a computational region, the computational complexity will be increased, and the grid element will be enlarged, the overall computational accuracy will be reduced. Therefore, in the process of extracting flood disaster information, the temporal continuity of spatiotemporal video sequence of flood motion will be fully considered, and the video sequence will be manually divided into two different categories. After spatiotemporal slicing and clustering, the moving samples are used to correspond to their sub-shots, and a key frame is extracted from them according to the preset rules. The extracted key frames need to be satisfied:

$$\text{Completness}\left(v\right) = \frac{\left|O^v\right|}{\max\limits_{k\in\pi}\left|O^k\right|} \tag{9}$$

Among them, π represents the optional range of the motion video block V in the temporal and spatial sequence, while O^v and O^k represent the number of targets containing video frames V and K in the current video sequence, respectively. The integrity of the extraction content of flood spatiotemporal motion key frame can be guaranteed through the constraint of Eq. (4).

So far, the data dynamic acquisition design of two-dimensional flood routing mathematical model has been completed

2.2. Flood disaster data preprocessing

Ensure the integrity of data in order to output the key frames of flood spatial-temporal movement in the form of still images, improve the accuracy of dynamic feature extraction of flood disaster data, and preprocess flood disaster data. The preprocessing of flood spatial-temporal moving image is realized by moving object detection, image enhancement and image normalization.

2.2.1. Moving target detection

The key problem of temporal and spatial motion feature extraction is to detect high quality temporal and spatial motion images of flood, in which background subtraction and image extraction are involved. The concrete moving object detection method is shown in Fig. 3.

According to Fig. 3, let $P_j(x,y)$ be the pixel value of the video image at position (x,y), and then use the background subtraction technology to extract the target foreground image in the image. Suppose $f_i(x,y)$ is the extracted spatiotemporal flood spatiotemporal motion image, and then substitute the background model of Eqs. (8) into (9), and the foreground flood spatiotemporal motion image of the moving video image can be obtained:

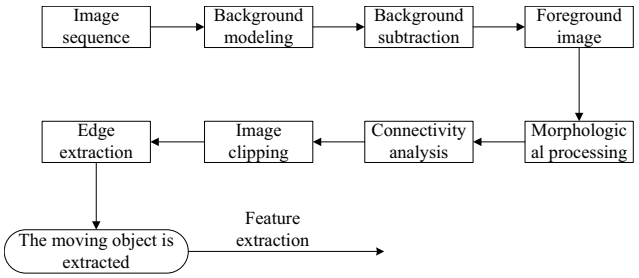

Fig. 3. Flow chart of flood temporal and spatial movement detection.

$$d_i(x,y) = \left| f_i(x,y) - B(x,y) \right| \tag{10}$$

It can pave the way for the extraction of temporal and spatial movement characteristics of flood under temporal and spatial weight.

2.2.2. Image enhancement processing of flood spatiotemporal motion

The enhancement of spatial-temporal motion image of flood has experienced two steps. The first step is to take the foreground image in the image as the processing object to reduce the noise. The step is to avoid the noise and target image being enhanced simultaneously, and affect the definition of the spatial and temporal motion image of flood; Gabor filter is selected to enhance the image sharpening and the spatial-temporal motion image of flood is enhanced by using the filter in the second step. Assuming that the noise reduction filter of the spatial-temporal motion image of flood is $h(x,y)$, then the noise elimination image is obtained by convolution of the noisy image. The process of noise elimination can be described as follows:

$$f(x,y) = d_i(x,y) \times h(x,y) \tag{11}$$

The best resolution can be obtained in both spatial domain and frequency domain.

2.2.3. Image normalization

The position of the water area is in a state of constant change in the process of movement [13–14] in the flood spatial-temporal motion image, so it is necessary to normalize the image to a uniform size, and specify the water movement area in the same central position, so as to realize the water position adjustment in all images. It is convenient for the subsequent extraction of corresponding image features in flood spatiotemporal motion image [15]. Firstly, the edge of water in video sequence is detected, as x_{min}, x_{min}, y_{min}, and y_{min}, Eq. (12) is used to determine the center of the moving water area.

$$\begin{cases} x = \dfrac{(x_{\min} + x_{\max})}{2} \\ y = \dfrac{(y_{\min} + y_{\max})}{2} \end{cases} \tag{12}$$

The image is cut to a fixed size, and the whole water moving area can be preserved in the cut image.

All variables are recursively processed, and one redundant feature vector is removed every cycle, so that the remaining eigenvectors are obtained. Then repeat the operation to calculate other eigenvectors, and finally get the list of transient stability characteristics of the model.

According to the principle of feature extraction of support vector, the extraction objective function is as follows:

$$W = \frac{1}{n}\sum_{h}^{h=0} \frac{\cos 2\pi h}{n} \tag{13}$$

where n is the number of model features; h is the signal spectrum amplitude.

The final state evaluation model based on the objective characteristic function of transient stability and the evaluation error rate is concluded as follows:

$$\gamma = \frac{\alpha + k + u}{\epsilon_1 + \epsilon_2} \tag{14}$$

where α represents the correct resolution; k represents the target statistical value; u represents the area of the integral, ϵ_1, ϵ_2 represented by the eigenvector represents the error rate.

So far, the preprocessing of flood disaster data has been completed, laying a foundation for accurate extraction of dynamic characteristics of flood disaster data.

3. Improved Gabor wavelet transform to extra CT dynamic characteristics of flood disaster data

3.1. Gabor wavelet transform method

Wavelet transform algorithm is also known as CWT. Wavelet transform inherits and develops the idea of short-time Fourier transform localization, and overcomes the shortcomings of window size not changing with frequency. It can provide a "time-frequency" window that changes with frequency. It is an ideal tool for time-frequency analysis and processing of signals. Its main feature is that it can fully highlight the characteristics of some aspects of the problem through transformation, can analyze the localization of time (space) frequency, and gradually refine the signal (function) at multiple scales through expansion and translation operations, so as to finally achieve the time subdivision at high frequencies and frequency subdivision at low frequencies, which can automatically adapt to the requirements of time-frequency signal analysis, so as to focus on any details of the signal. Physicists transform wavelet functions into signals of different scales according to the actual situation according to the theory of Wavelet transform and the feature that functions can move and flex freely. The calculation formula of transform is as follows:

$$\mathrm{WT}_x(a,\tau) = \frac{1}{\sqrt{a}} \int_{-\infty}^{\infty} \frac{x(t)\varphi(t-\tau)}{a} dx \tag{15}$$

Among them, represents different scales of the function; ϕ represents the extreme value of the function; τ represents the length of the function movement displacement; $x(t)$ represents the signal to be analyzed for the wavelet transform function.

The corresponding frequency-domain function formula of wavelet transform function is as follows:

$$\mathrm{WT}_x(a,\tau)=\frac{\sqrt{a}}{2\pi}\int_{-\infty}^{\infty}X(\omega)\varphi(a\omega)dx \tag{16}$$

where $X(\omega)$ represents the Fourier function after wavelet transform; ω represents the phase of the function.

In the application of wavelet transform algorithm, the application of the algorithm must meet certain functional conditions [16]. The smaller the scale of the wavelet transform function is, the smaller the redundant information is, the higher the efficiency of the transform is, and the larger the frequency domain of the corresponding function is.

3.2. Dynamic feature extraction based on improved Gabor wavelet transform

A Gabor feature based on orientation pre-classification is proposed based on the original Gabor feature in this paper, and the fuzzy direction of stroke calculated by fuzzy set is introduced.

First, the center frequency of Gabor function is determined by counting the actual stroke width. 0U = 0.08, 0.1, 0.125, and the corresponding stroke width is 6, 5, 4. In order to compute conveniently, it is approximately considered that the distribution of image strokes is similar in all directions, which makes it advantageous for the Gabor function to select the stroke direction. On this basis, the parameters are adjusted to pre-classify the stroke direction before filtering. The process is as follows:

First, convert the object to be identified to a binary image, and then calculate the loss function for each pixel using the sober operator:

$$L=hL_1+\gamma L_2+\varphi L_3 \tag{17}$$

where L_1 represents the amount of stroke width loss in each direction; L_2 represents the amount of loss of the stroke direction selection coefficient; L_3 represents the loss of the actual stroke width and the pre classification threshold of other targets; γ and ϕ represent the weight index of the two parts of loss value after the balance treatment. H is the gray value.

The above formula represents the specific gravity of the actual stroke width in the overlapping region K^S_2. The function can reduce the loss of some parts. After the direction of each pixel point is obtained, the angle of the first and fourth quadrants is divided into k-direction sets, which satisfies the requirements:

$$L_1=\frac{k\sum_{S\in\rho^+}\mathrm{Smooth}\left(A^S,K_1^S\right)}{\left|\rho^+\right|} \tag{18}$$

where ρ^+ a positive sample is set; A^S represents the actual stroke width of the algorithm; K^S_1 represents the actual target box with the maximum value of IOU for parameter S. The Smooth(*) function is used to obtain the loss relationship between A^S and K^S_1, and the average result of positive sample loss is taken as the final value of loss.

Then, because of the offset of character position, inclination and deformation, the fuzzy set theory is used to calculate the fuzzy direction of strokes, which can improve the robustness of the feature. Every pixel is divided into a set of directional values, and several sets are obtained to form a fuzzy direction set:

$$L_2=\frac{\sum_{S\in\rho^+}\mathrm{Smooth}\left(\log\left(A^S,K_2^S\right)\right)}{\left|\rho^+\right|} \tag{19}$$

$$\log(A,K)=\frac{\mathrm{area}(A\cap K)}{\mathrm{area}(K)} \tag{20}$$

(A,K) represents the direction of the pixels whose coordinates are A and K.

The normalized image whose size is $N \times N'$ is divided into $M \times M$ grid sets so that each grid set is equal in size. Based on this normalized image, the membership degree of all pixels to K fuzzy orientation sets is calculated, and the corresponding Gabor features are extracted in each grid according to the above calculation:

$$L_3=\frac{\sum_{i\neq j}\mathrm{Gabor}\left(\mathrm{IOU}\left(A^{S_i},A_2^{S_j}\right)\right)}{\sum_{i\neq j}\left[\mathrm{IOU}\left(A^{S_i},A_2^{S_j}\right)>0\right]+c} \tag{21}$$

Among them, c represents the adjustment parameter of dynamic characteristics. Set $f(\alpha_{max})$ as the migration limit function, calculate the expected value, variance and coefficient of variation of each feature, and calculate and analyze the importance of the feature matching index. Therefore, suppose that the expected value of the ird indicator is $\bar{z}_i$, the variance of the i-th indicator is S_i^2, and the coefficient of variation of the i-th indicator is c_i. j represents the indicator level, p_{ij} represents the j-rd level measurement of the i-nd indicator, and z_j represents the measurement value [17–19], that is, z_j = 0.2, 0.4, 0.6, 0.8, 1 represents unimportant, general, more important, very important and very important, respectively, The higher the importance, the higher the integrity and accuracy of the extraction.

The overall flow of dynamic feature extraction of flood disaster data based on improved Gabor wavelet transform is shown in Fig. 4.

The design of flood disaster data dynamic feature extraction method based on improved Gabor wavelet transform is realized through the above contents. High-quality data is provided for the introduction of improved Gabor wavelet transform to extract flood disaster data dynamic features by collecting flood disaster data [20] and preprocessing the data, so as to improve the extraction quality.

4. Experiment

4.1. Experimental preparation

The meteorological data needed are obtained from the daily precipitation data of meteorological stations from

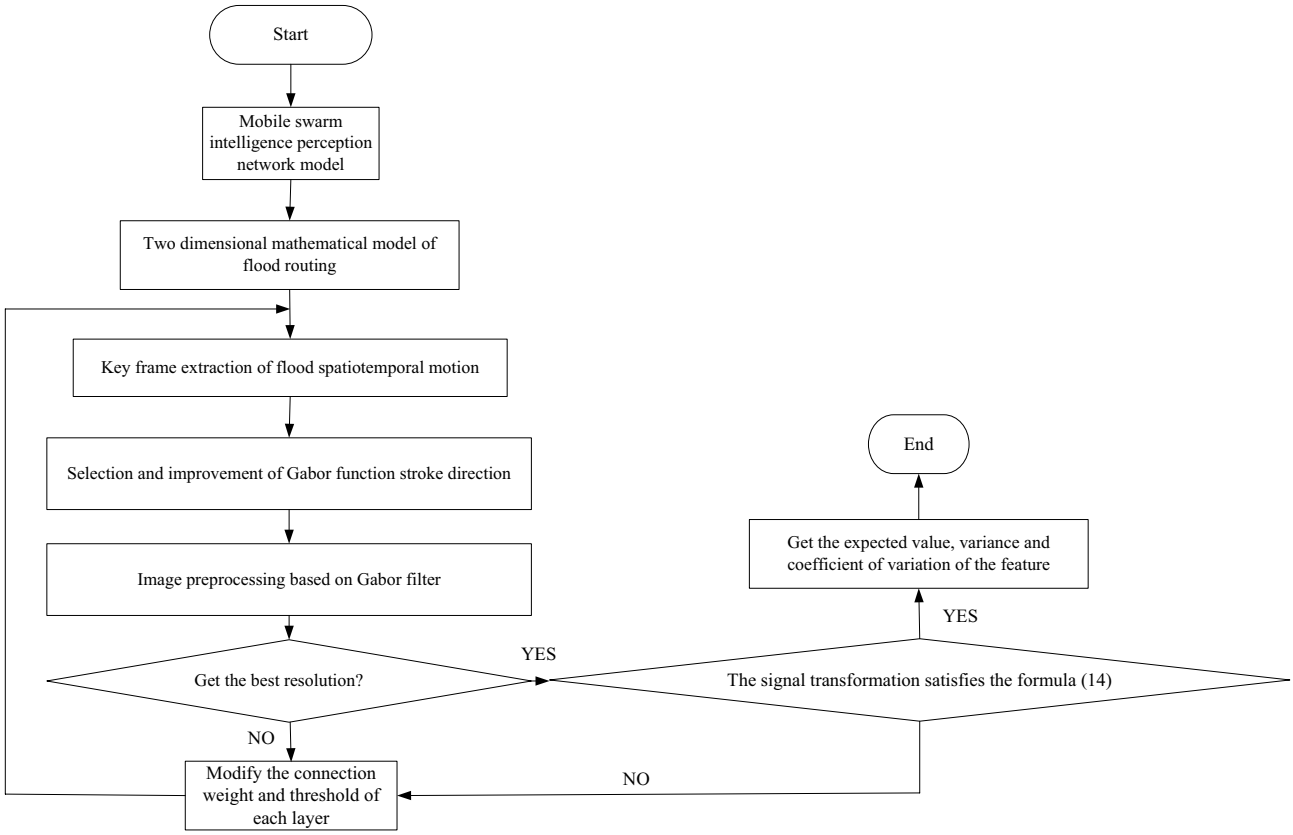

Fig. 4. Extraction process of dynamic characteristics of flood disaster data.

2010 to 2020 and the data obtained from the relevant information of the China Meteorological Data Network (http://data.cma.gov.cn/)in this experiment, and the data are connected with the model through the application programming interface; the disaster information is obtained from the data of the 2010–2020 Census of Flood and Waterlogging Disasters; And the social economic information is obtained from the statistical yearbook published by the Statistics Bureau, in which the data is obtained from the case according to the relevant information of the network of the Statistics Bureau of a province.

Initialization Data Setting: Taking the coordinate of the dyke as the origin and the flood water level as the starting point, the user can modify the starting point coordinate, flood water level and flood flow rate conveniently according to the need of simulation. The basic parameters such as the source point of flood simulation and flood water level are input in the model condition, and the model parameters and the original data are input in the observation data of hydrological station.

Table 1 shows the experimental data.

The flood simulation can be carried out and displayed in the three-dimensional visual window after the flood simulation parameters are input, as shown in Fig. 5.

In Fig. 5, the spectral characteristics of water body are determined by its own properties, but different water states also have different spectral characteristics, which makes it different from the real water body; Compared with other ground objects, the water body has strong absorption to the incident solar energy in the whole spectral range, and the remote sensing shows weak reflectivity in the whole spectral range, especially in the near-infrared, mid infrared and short infrared parts, the water body almost absorbs all the incident energy, so the reflection energy of the water body in these bands is very small. On the contrary, soil, buildings and vegetation have higher reflectance, which makes water body different from other features.

4.2. Calculation formula of experimental parameters

The calculation formula of each parameter is as follows:

- The momentum equations of water flow along m direction are as follows:

$$\frac{\partial h\bar{u}}{\partial t}+\frac{\partial h\bar{u}^2}{\partial m}+\frac{\partial h\overline{uv}}{\partial n}=f\bar{v}h-gh\frac{\partial \eta}{\partial m}-\frac{h}{p_0}\frac{\partial p_a}{\partial m}-\frac{gh^2}{2p_0}\frac{\partial p}{\partial m}+\frac{\tau_{sm}}{p_0}-\frac{\tau_{bm}}{p_0}-\frac{1}{p_0}\left(\frac{\partial_{S_{mm}}}{\partial m}+\frac{\partial_{S_{mn}}}{\partial n}\right)+\frac{\partial}{\partial m}\left(hT_{mm}\right)+\frac{\partial}{\partial n}\left(hT_{mn}\right)+h_{u_s}s \tag{22}$$

Among them, η represents the river bottom elevation; *d* is still water depth; *f* is the coefficient of Coriolis force; *g* is the acceleration of gravity;

Among them, ω represents the rotation velocity of the earth; ω represents the local dimension;

Table 1
Description of relevant parameters

Project	Parameter
Coordinates of starting point x	515,987.140
Coordinates of starting point y	554,987.357
Coordinates of starting point z	128.16875
Flood water level	136.284 m
Flood velocity	20 m/s
Sectional area	10 km^2
Upper tension water capacity	10 mm
Lower tension water capacity	65 mm
Deep tension water capacity	85 mm
Conversion coefficient of evapotranspiration capacity	0.93
Power of storage capacity of tension water	0.2
Deep evapotranspiration coefficient	0.10
Proportion of impervious wave area	0
Dissipation coefficient of flow in deep soil	0.9
Regression coefficient of underground reservoir	0.9
Discharge coefficient of free water storage reservoir in topsoil to groundwater	0.4
Flow coefficient of free water storage reservoir in topsoil to soil flow	0.4

Fig. 5. Dynamic simulation model of flood disaster in experimental area.

- The momentum equations of water flow along n direction are as follows:

$$\frac{\partial h\bar{v}}{\partial t}+\frac{\partial \overline{huv}}{\partial m}+\frac{\partial h\bar{v}^2}{\partial n}=-f\bar{u}h-gh\frac{\partial \eta}{\partial n}-\frac{h}{\rho_0}\frac{\partial \rho_a}{\partial n}-\frac{gh^2}{2\rho_0}\frac{\partial p}{\partial n}+\frac{\tau_{sn}}{\rho_0}-\frac{\tau_{bn}}{\rho_0}-\frac{1}{\rho_0}\left(\frac{\partial_{S_{mm}}}{\partial m}+\frac{\partial_{S_{nn}}}{\partial n}\right)+\frac{\partial}{\partial m}\left(hT_{mn}\right)+\frac{\partial}{\partial n}\left(hT_{nn}\right)+h_{v_s}s \tag{23}$$

Among them u_x and v_x represent the flow velocity of source term; S_{mm}, S_{nn} and S_{mn} represent the stress component, respectively; s represents the amount of source traffic.

Combined with the above formula, a three-dimensional mathematical model of visual scheduling is constructed.

$$\frac{\partial h}{\partial t}+\frac{\partial h\bar{u}}{\partial m}+\frac{\partial h\bar{v}}{\partial n}=hs \tag{24}$$

where t represents time, m, n represents the coordinates of the Cartesian coordinate system, u, v represents the velocity component in the direction and direction m, n, respectively; ρ_0 represents the relative density of water; h is the sum of η, d, representing the total water depth.

4.3. Performance analysis

It has the characteristics of suddenness, short duration, and great harm and most prone to occur because flood disaster is a kind of sudden event, the evaluation cycle of flood disaster model is more than 2 d. The index importance and positive sample loss value of flood disaster data extraction at different times are set as test indexes, and the method in this paper is compared with the method of [6], the experimental results of the three models are given in Table 2.

According to the experimental data in Table 2, within 15 d, the importance of the index of this method is higher than that of the other two literature methods, which promotes the execution efficiency of the whole model greatly. This is because this method improves Gabor wavelet transform algorithm and recursively processes all variables, one redundant feature vector is removed every period. According to the list of transient stability characteristics of the model, the final state evaluation model is concluded, and the normalization of the image is completed, and the importance and availability of the indicators are expanded.

Taking the initial flood parameters as the control, and the results of the positive sample loss rate of flood disaster data applied by different methods are tested based on the simulation results. The actual application performance

Table 2
Comparison results of index importance of different methods

Time (d)	Index importance (%)		
	Method of this paper	Methods of Li [3]	Methods of Zhao et al. [4]
2	200.00	91.35	95.59
3	99.95	94.52	92.35
4	95.24	94.25	90.57
5	97.53	92.99	91.29
6	95.24	94.25	92.79
7	99.52	94.52	95.39
8	99.25	95.20	95.24
9	97.24	95.95	94.25
10	95.22	95.35	93.97
11	97.74	94.97	92.24
12	95.97	95.59	93.25
13	95.49	95.25	94.25
14	94.79	90.74	92.74
15	98.25	95.02	94.25

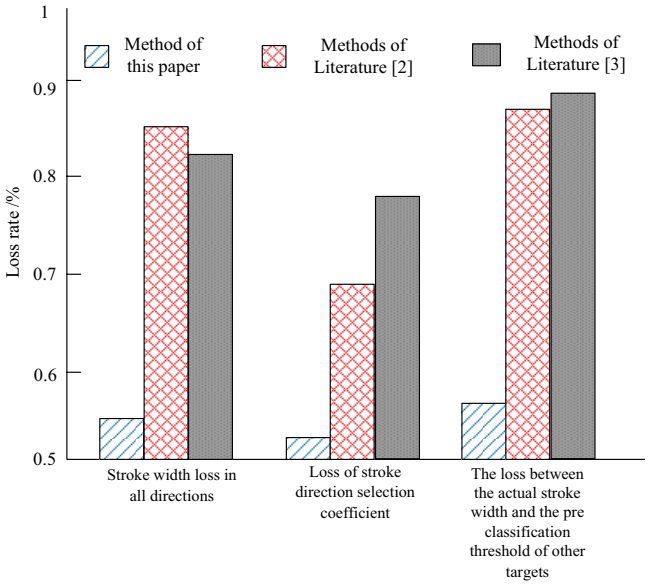

Fig. 6. Comparison of positive sample loss rate of flood disaster data with different methods.

of the method is evaluated. The test results are shown in Fig. 6.

Fig. 6 shows that compared with other methods, the fuzzy set theory can improve the robustness of the feature. Every pixel is divided into several sets according to the direction value, and the initial stroke width and the actual stroke width fit well, and the loss rate of the positive stroke is lower, so its practical application performance is ensured.

5. Conclusion

Flood and waterlogging are a kind of sudden natural disaster. Most of them are sudden and harmful. In the process of taking corresponding prevention and control measures for flood and waterlogging disasters, human beings mainly divide them into four stages: flood control and comprehensive management, flood monitoring and forecasting and early warning, flood disaster monitoring and flood control and rescue, comprehensive assessment of flood disaster and auxiliary decision-making analysis of disaster reduction. The work of flood and waterlogging disaster monitoring is closely related to the latter two stages, and the data processing and feature extraction in the process directly relates to the formulation and implementation of disaster reduction measures as well as the disaster assessment and disaster relief after the disaster. In this paper, an improved Gabor wavelet transform based method is proposed to extract the dynamic features of flood disaster data. The innovation of the method is to build a two-dimensional flood routing mathematical model based on mobile group intelligence perception network, and to set the boundary conditions and parameters of flood disaster region, so that the stroke deformation and low-resolution characters have better adaptability. The fuzzy set theory is used to compute the fuzzy direction of stroke, and the fuzzy stroke width of Gabor function is used to integrate the fuzzy stroke width in multiple directions.

For the remote sensing of ground objects, the absorption band must be avoided, and the atmospheric window band, such as visible light, near infrared, short infrared, thermal infrared and microwave band, should be chosen. Therefore, in the future, the compensation of atmospheric influence must be taken into account and the correction must be made when quantitative remote sensing is carried out, that is, high quality remote sensing images of flood disasters are obtained by radiometric correction.

Acknowledgments

Science and Technology Program of Gansu Province: Application of Key Technologies on Mountain Flood Disaster Monitoring and Warning in Gansu Section of Yellow River Based on Big Data (No. 22YF7FA131).

References

[1] T.K. Ghosh, F. Jakobsen, M. Joshi, K. Pareta, Extreme rainfall and vulnerability assessment: case study of Uttarakhand rivers, Nat. Hazards, 99 (2019) 665–687.
[2] S. Wang, K. Zhang, L. Chao, D. Li, X. Tian, H. Bao, G. Chen, Y. Xia, Exploring the utility of radar and satellite-sensed precipitation and their dynamic bias correction for integrated prediction of flood and landslide hazards, J. Hydrol. (Amsterdam), 603 (2021) 126964.1–126964.15.
[3] C.G. Li, 3D flood simulation analysis based on ArcGIS, Metall. Collect., 4 (2021) 27–28.
[4] Q. Zhao, P. Zhong, G. Liu, X. Wan, Y. Wang, Research on dynamic control domain of flood control Level of Hekoucun reservoir based on forecasting operation, Water Resour. Power, 30 (2019) 62–65.
[5] F. Maritsch, I. Cil, C. McKinnon, J. Potash, N. Baumgartner, V. Philippon, B.G. Pavlova, Data privacy protection in scientific publications: process implementation at a pharmaceutical company, BMC Medical Ethics, 23 (2022) 1–10.

[6] R.H. Khokhar, F. Iqbal, B.C.M. Fung, J. Bentahar, Enabling secure trustworthiness assessment and privacy protection in integrating data for trading person-specific information, IEEE Trans. Eng. Manage., 68 (2021) 149–169.
[7] K. Yu, K. Kashima, C. Ming, Modular control under privacy protection: fundamental trade-offs, Automatica, 127 (2021) 109518.1–109518.11.
[8] T. Zheng, The continuity equation of the Gauduchon metrics, Pac. J. Math., 310 (2021) 487–510.
[9] M.A. Dayananda, A direct derivation of Fick's law from continuity equation for interdiffusion in multicomponent systems, Scr. Mater., 210 (2022) 114430.1–114430.5.
[10] H. Ki, Unified momentum equation approach for fluid–structure interaction problems involving linear elastic structures, J. Comput. Phys., 415 (2020) 109482.1–109482.19.
[11] C.T. Nguyen, V.N. Bao, Application of flood vulnerability index in flood vulnerability assessment: a case study in Mai Hoa Commune, Tuyen Hoa District, Quang Binh Province, Sustainable Water Resour. Manage., 5 (2019) 1917–1927.
[12] P.J. Robinson, W.J. Wouter Botzen, Determinants of probability neglect and risk attitudes for disaster risk: an online experimental study of flood insurance demand among homeowners, Risk Anal., 39 (2019) 2514–2527.
[13] Z. Wu, Y. Shen, H. Wang, M. Wu, Assessing urban flood disaster risk using Bayesian network model and GIS applications, Geomatics Nat. Hazards Risk, 10 (2019) 2163–2184.
[14] K. Zhang, Md H. Shalehy, G.T. Ezaz, A. Chakraborty, K.M. Mohib, L. Liu, An integrated flood risk assessment approach based on coupled hydrological-hydraulic modeling and bottom-up hazard vulnerability analysis, Environ. Modell. Software, 148 (2022) 105279–105294.
[15] G. Yue, Y. Pan, Intelligent inspection of marine disasters based on UAV intelligent vision, J. Coastal Res., 93 (2019) 410–416.
[16] C.A. Langston, Phased array analysis incorporating the continuous wavelet transform, Bull. Seismol. Soc. Am., 111 (2021) 2780–2798.
[17] M.N. Aidi, The influence of precipitation, stream discharge, and physiographic factors on flood vulnerability at Cimanuk Riverwest Java, Indonesia, J. Sustainability Sci. Manage., 14 (2019) 125–136.
[18] Y. Zhang, Y. Wang, Y. Chen, F. Liang, H. Liu, Assessment of future flash flood inundations in coastal regions under climate change scenarios – a case study of Hadahe River basin in northeastern China, Sci. Total Environ., 69 (2019) 1–3.
[19] J. Oliver, X.S. Qin, H. Madsen, P. Rautela, G.C. Joshi, G. Jorgensen, A probabilistic risk modelling chain for analysis of regional flood events, Stochastic Environ. Res. Risk Assess., 33 (2019) 1057–1074.
[20] K.H.V. Durga Rao, S. Alladi, A. Singh, An integrated approach in developing flood vulnerability index of India using spatial multi-criteria evaluation technique, Curr. Sci.: A Fortnightly J. Res., 117 (2019) 80–86.